Sensors & Actuators: B. Chemical 369 (2022) 132276

Contents lists available at ScienceDirect

Sensors and Actuators: B. Chemical

journal homepage: www.elsevier.com/locate/snb

An addressable electrowetting valve for centrifugal microfluidics

Yanming Xia [a,b], Chao Song [b], Yingchao Meng [b], Peng Xue [b,c], Andrew J. deMello [b], Quan Gao [b,d], Stavros Stavrakis [b], Shenglin Ma [a,*], Xiaobao Cao [b,e,**]

[a] Department of Mechanical & Electrical Engineering, Xiamen University, Xiamen, China
[b] Institute for Chemical and Bioengineering, ETH Zürich, 8093 Zürich, Switzerland
[c] Institute of Biophysics, Chinese Academy of Sciences, Beijing, China
[d] Institute of Robotics and Intelligent Systems, ETH Zürich, 8006 Zürich, Switzerland
[e] Guangzhou Laboratory, 510320 Guangzhou, Guangdong, China

ARTICLE INFO

Keywords:
Centrifugal microfluidics
Valve
Electrowetting

ABSTRACT

Centrifugal microfluidic platforms aim to integrate and perform complex biological and chemical processes within disc-like substrates and valving through centrifugal forces and the Coriolis effect. Although the integration of active valves within such system can be used to enhance fluid control, the ability to fabricate and integrate addressable valves within centrifugal platforms remains a significant challenge. To address this issue, herein, we present and test an addressable electrowetting centrifugal (EWC) valve. The EWC valve comprises a hydrophobic burst valve, integrated side electrodes and a dielectric layer between the microfluidic channel and electrode structures. The burst valve is made from a hydrophobic material able hold a specified pressure. Specifically, application of an external electric field is used to alter the valve wettability, making the valve more hydrophilic, decreasing the threshold pressure and triggering the opening of the valve. To assess valve performance, we investigate the influence of electric properties and channel geometry on valve response and then demonstrate multiple operations on different fluid samples. Finally, and to highlight the utility of EWC valves, we demonstrate the detection and analysis of CD4 human immune cells.

1. Introduction

Microfluidic systems allow the control of fluid flow on sub-nL scales, providing numerous advantages when performing chemical or biological experiments. In simple terms, microfluidic systems are able to process small sample volumes with ease, perform and automate multiple functionalities in an integrated manner and control both heat and mass transport with unrivaled precision [1]. Centrifugal microfluidic systems, also commonly known as lab-on-a-disc systems, integrate a variety of functional operations within a spinning disc format. Driven by a single motor, centrifugal microfluidic platforms are simple to control, do not require external pumps to drive the fluid [2,3]. Unsurprisingly, centrifugal microfluidic systems have been used in a range of biological applications, including immunoassays [4,5] and nucleic acid analysis [6,7].

In all centrifugal microfluidic platforms, rapid rotation of the device generates a centrifugal force that drives the fluid (contained within microfluidic channels) outwards from the center and towards the boundary. Whilst this is simple to achieve, basic centrifugal microfluidic platforms lack flexibility in their ability to precisely control fluid flow when compared to more traditional microfluidic technologies. This in turn limits the number of distinct fluidic operations that can be performed in an integrated and automated manner. Accordingly, the ability to integrate valves within centrifugal microfluidic platforms is important in exerting better fluid control and allowing the performance of complex experimental workflows. Valves within centrifugal platforms are typically classified as being either passive or active in nature [2]. The "burst valve" is the most commonly used passive valve due to its simple structure and easy integration [8–10]. In its simplest embodiment, a burst valve consists of an expanding geometry or hydrophobic surface modification within a microchannel, with fluid only being able to pass through the valve if the applied pressure overcomes surface tension. Examples of more sophisticated burst valves include elastomeric membrane valves integrated into a disc [11], and 3D slope valves, which

* Corresponding author.
** Corresponding author at: Institute for Chemical and Bioengineering, ETH Zürich, 8093 Zürich, Switzerland.
E-mail addresses: mashenglin@xmu.edu.cn (S. Ma), xcao@ethz.ch (X. Cao).

https://doi.org/10.1016/j.snb.2022.132276
Received 22 February 2022; Received in revised form 26 April 2022; Accepted 24 June 2022
Available online 28 June 2022

allow for precise and sequential fluid control through both centrifugal and gravitational forces [12]. Whilst such technical innovations have enhanced fluid control within centrifugal platforms, fluid manipulation using passive valves is primarily controlled by the spinning speed of the entire disc, making independent valve operation almost impossible. Active valves overcome this limitation and allow more precise and bespoke fluid control [13]. For example, membranes can be used in an "active" manner under rotation. Deflection of a membrane can be induced by various stimuli, including laser heat-melting [14–16], chemical dissolution [17], mechanical deformation [18,19], thermal expansion [20] and mechanical twisting [21]. Although useful, such valves can often contaminate the contained sample and their relatively large cross-sectional dimensions hinder facile integration. And the valve needs to move to certain place to receive the actuation from external stimuli, which increase actuation time and bring difficulty to operate valves in parallel. To overcome these limitations, Wang and co-workers have reported a series of centrifugal valves, which are actuated by the vertical movement of a spring connected to a mechanical system such as a fly-ball [22–24], a wedge [25], or a sliding weight [26]. Finally, Kim et al. reported a range of diaphragm valves comprising an elastic epoxy film embedded in a 3D-printed push-and-twist valve, which is actuated by a simple automatic driving unit [27,28]. Again, whilst useful, their large footprint (typically mm-scale) prohibits multiplexing.

Whilst all the aforementioned valves have shown some utility within centrifugal platforms, there remains a need for active valves that can be integrated in a facile manner, whilst requiring only minimal peripheral control architecture. To this end, we present an addressable electrowetting centrifugal (EWC) valve formed when two electrodes are located across a narrow microfluidic channel made from a hydrophobic material. When a voltage is applied across the electrodes, the channel wall is made more hydrophilic, allowing fluid transport through the channel under the influence of the centrifugal force. Significantly, valves may be rapidly and selectively opened through (remote) control of the applied electric field. In addition to assessing the performance of the EWC valves, we showcase their utility through the implementation of a fluorescence-linked immunosorbent assay for the detection of CD4 cell antigens, important biomarkers of HIV infection [29,30].

1.1. Operating principle of the EWC valve

A centrifugal microfluidic platform integrating 12 EWC valves is shown in Fig. 1a. In its simplest embodiment, an EWC valve comprises a hydrophobic burst valve flanked by two electrodes and a dielectric layer positioned between the microfluidic channel and electrodes. The burst valve acts to hold the flow at a narrow channel cross-section due to surface tension, and will open only when the pressure exceeds a certain threshold (Fig. 1b) [8–10,31,32]. To refine this pressure driven mechanism, we use an electric field to trigger valve opening in a sensitive and rapid manner. Specifically, under the application of electric field, the inter-electrode surface changes from hydrophobic to hydrophilic by surface charging. This process "opens" the valve, allowing fluid transport through the narrow channel under a centrifugal force (Fig. 1c) [33–36]. For a rotating microfluidic device, the centrifugal pressure is given by,

$$P = \rho R \Delta r \left(\frac{60N}{2\pi}\right)^2 \quad (1)$$

Here, P is the centrifugal pressure, ρ is the fluid density, R is the distance from the centrifugal center, Δr is the distance between the inner radial point and outer radial point of the liquid plug and N is the rotational speed (round per minute). These parameters are highlighted in Fig. 1b.

It is important to note that independent valve control can be achieved by connecting each valve via a slip ring [37]. However, such an approach does limit the number of valves that can be integrated per device due to the limited channels of the slip ring. Accordingly, a PCB board (with power supplied through a slip ring) integrating a WiFi module is used to control voltage switching on each valve. It should be noted that the patterned electrodes on the centrifugal microfluidic device are connected to the PCB board via spring electrodes installed on the control board. A microfluidic device integrating 4 EWC valves is presented in Fig. 1d.

2. Materials and methods

2.1. Chip fabrication

The workflow for the fabrication of centrifugal microfluidic devices is presented in Fig. 2. First, a 200 nm thick chromium layer is deposited on a glass slide (Menzel-Glaser, Braunschweig, Germany) using an Explorer 14 Sputtering System (Denton Vacuum, Moorestown, USA) (Fig. 2a). Next, a 1.4 μm layer of AZ5214 positive photoresist

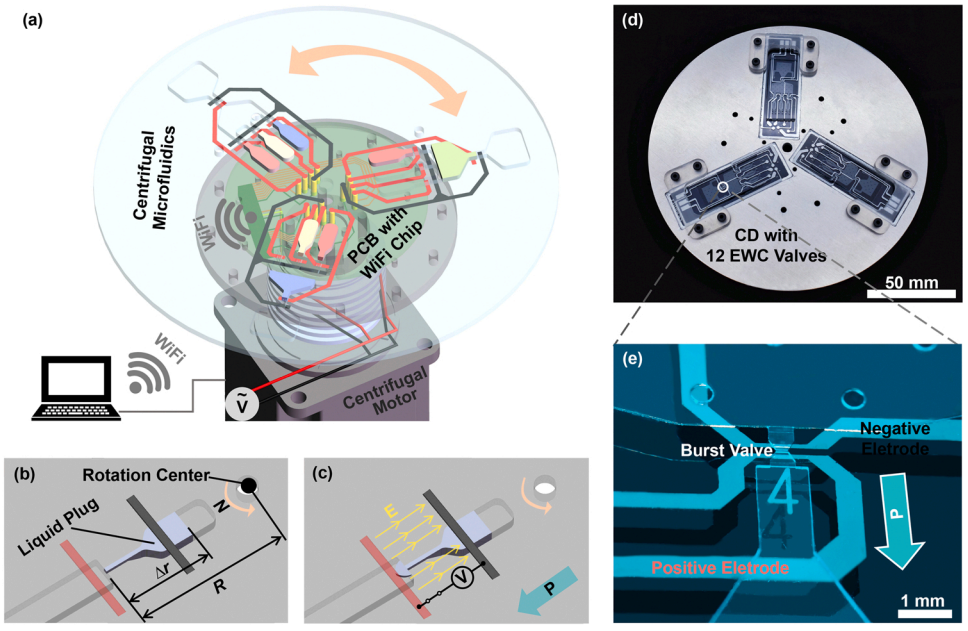

Fig. 1. Centrifugal microfluidic platform integrated with electrowetting valves. (a) Schematic of the entire centrifugal platform integrating 12 electrowetting valves. (b) Fluid under a certain centrifugal pressure is held by the narrow channel of burst valve, and schematic of its centrifugal pressure calculation parameters of Eq. (1). (c) Subsequent fluid transport through the narrow channel due to centrifugal pressure and the application of an electric field. (d) Top view image of a centrifugal microfluidic chip containing 12 EWC valves. (e) Detailed image of an EWC valve.

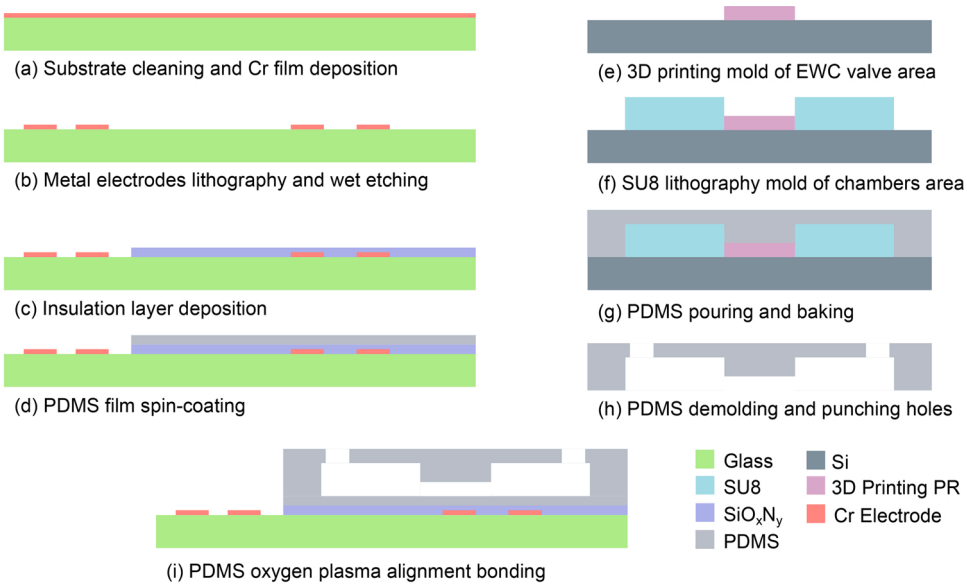

Fig. 2. Fabrication process of centrifugal microfluidic devices integrated with EWC valves.

(MicroChem, Round Rock, USA) is spun on top of the chromium layer and photolithographically patterned using an MA6 mask aligner (SUSS, Munich, Germany). The exposed regions of the chromium layer are then wet etched using a TechiEtch Cr01 etchant (MicroChem, Round Rock, USA) to yield the desired metal electrode patterns (Fig. 2b). Subsequently, a 500 nm thick SiO_xN_y insulating layer is deposited on top of the electrodes using a PECVD 80 + plasma-enhanced chemical vapor deposition system (Oxford Instruments, Bristol, UK) (Fig. 2c). Next, a 10:1 mixture of Sylgard 184 PDMS (Dow Corning, Midland, USA) is spin-coated onto the SiO_xN_y layer at 1200 rpm for 50 s to yield a 70 μm-thick elastomer layer (Fig. 2d).

Microfluidic device masters were fabricated in stages via 3D printing and lithography. Valve regions were fabricated using a two-photon stereolithography printer (Nanoscribe GmbH, Stutensee, Germany) with a 63 × objective and an IP-Dip photoresist (Nanoscribe GmbH, Stutensee, Germany). The resulting structure was developed for 15 min in SU-8 Developer (MicroChem, Round Rock, USA) and then rinsed in isopropyl alcohol for 5 min (Fig. 2e). Subsequently, larger features were produced using conventional photolithography of an SU-8 photoresist. A 50 μm thick layer of SU-8 2050 (MicroChem, Round Rock, USA) was spin-coated on the wafer, and baked for 2 min at 65 ℃ and then 7 min at 95 ℃. The photoresist was aligned with the 3D printed structure and exposed using an MA6 mask aligner (SUSS, Munich, Germany). After post baking for 1 min at 65 ℃ and 6 min at 95 ℃, the wafer was developed for 6 min in SU-8 Developer, rinsed in isopropyl alcohol and then baked at 200 ℃ for 15 min (Fig. 2f).

Subsequently, a 10:1 mixture of Sylgard 184 PDMS (Dow Corning, Midland, USA) was poured over the master mold, cured at 70 ℃ for 4 h and then peeled off (Fig. 2g). After forming inlet and outlet ports using a hole-puncher (Technical Innovations, West Palm Beach, USA) (Fig. 2h), the structured PDMS substrate was aligned and bonded with the PDMS film (on the glass slide) after treating both surfaces in an EMITECH K1000X oxygen plasma (Quorum Technologies, Wealden, UK) (Fig. 2i).

2.2. Bioassay

Three separate reagents (CD4 antibody-bound magnetic beads, CD4 cell antigen and fluorophore-conjugated CD4 antibodies) were prepared and used for the detection of CD4 human immune cells. CD4 antibody-bound magnetic beads were prepared as follows. First, 10 mg/mL NHS activated magnetic beads (Thermo Scientific, Waltham, USA) were washed using 1 mM ice-cold hydrochloric acid and collected in a microcentrifuge tube. After removing the supernatant, 10 μL of 0.5 mg/mL CD4 Monoclonal Antibody GK1.5 (Invitrogen, Santa Clara, USA) was added to the tube and incubated with magnetic beads on a rotator for 2 h at room temperature. The CD4 antibody-bound beads were then washed using 0.1 M glycine (pH 2.0) twice, ultrapure water once, quenching buffer (3 M ethanolamine, pH 9.0) once and PBS buffer three times, respectively. Finally, 10 μL PBS was added to the tube to resuspend the solution. CD4 cell antigen was prepared as follows. First, 0.5 mg/mL solution was made by dissolving 5 μg Human CD4 His-tag Recombinant Protein antigen (Invitrogen, Santa Clara, USA) in 10 μL PBS as a storage solution. Then the storage solution was diluted into 10 μL 0.4 mg/mL, 0.3 mg/mL, 0.2 mg/mL, 0.1 mg/mL, 0.08 mg/mL, 0.06 mg/mL, 0.04 mg/mL and 0.02 mg/mL aliquots, respectively.

2.3. Experimental setup

A schematic of the entire centrifugal microfluidic platform is shown in Fig. S1. An ECMA-C10604SS drive motor (Delta, Hoofddorp, Netherlands) was fixed onto a homemade stage and used to control device rotation. A slip ring (used to connect a stationary system to a rotating system) was mounted on the shaft of the motor to allow electrical connection between the chip and power supply. External electric fields were generated using a 33210A function wave generator (Agilent Technologies, Santa Clara, USA) and amplified by a Model 2210 power amplifier (Trek, New York, USA). The EWC centrifugal microfluidic system was electrically connected via copper spring pins (Zhenghe, Dongguan, China) and physically fixed onto the chip holder with the PCB board. The control board received commands from the PC via the WiFi module. This allows precise control of the electric field applied to each valve and thus switching between “open’ and ”closed” states. Wireless connection between the computer and WiFi chip is achieved using the Mega 2560 open-source electronics platform (Arduino, Ivrea, Italy), with the computer sending valve control commands via NetAssist net-control software (Shanghai-Channel, Shanghai, China). To both record and assess the status of an EWC valve, a centrifugal trigger image acquisition system was established. Specifically, an FS-V11 fiber-optic sensor (Keyence, Osaka, Japan) was mounted alongside the microfluidic device and triggered once per rotation. A UI-3060CP high-speed, 2.3 megapixel camera (IDS, Obersulm, Germany) and 50 mm F1.4 camera lens (Canon, Tokyo, Japan) were used to record images of the microfluidic device when triggered by the optical sensor.

Due to image blurring when monitoring the rotating microfluidic

device, it was difficult to observe the movement of the fluid interface in the valve region during rotation. Accordingly, to probe the behavior of the liquid-air interface in the vicinity of the valve, we carried out a simulated experiment using a Ti-E inverted microscope (Nikon, Minato, Japan), with a Flow EZ pressure pump (Fluigent, Le Kremlin-Bicetre, France) being used to control the applied pressure (Fig. S2). A 10x Plan Achromatic Correction zoom lens (Nikon, Minato, Japan) was used to record the movement of the liquid interface via the UI-3060CP high-speed camera. The electric field is generated using a 33210A function wave generator and Model 2210 power amplifier. Surface wettability was assessed using a DSA optical tensiometer (Kruss, Hamburg, Germany).

3. Results and discussion

Four parameters, capillary channel width (w), capillary channel height (h), outlet angle (α) and outlet height of capillary channel (H) were initially investigated with regard to their impact on threshold pressure (Fig. S3). The threshold pressure was observed to decrease from 296.8 mBar to 60.2 mBar as the channel cross-section was increased from 5 × 5 μm to 30 × 30 μm, whilst maintaining an aspect ratio of 1 (Fig. S3b). The aspect ratio has a significant influence on threshold pressure repeatability, with the pressure RSD increasing from 6.6% to 32.9% when the aspect ratio increases from 1 (w: 5 μm, h: 5 μm) to 6 (w: 5 μm, h: 30 μm) (Fig. S3c). To ensure stable valve operation, all burst valves were fabricated with an aspect ratio of 1. Additionally, experiments indicated that there was no significant change in the threshold pressure when the outlet angle is varied between 15° and 90° (Fig. S3d). The outlet height also has minimal influence on the threshold pressure (Fig. S3e). Accordingly, the outlet angle and outlet height were set to 90° and 50 μm, respectively in all experiments.

We then compared the wettability of the PDMS surface with and without the application of an electric field, through measurement of the water contact angle. As can be seen in Fig. 3a, for a PDMS surface and without the application of an electric field, a contact angle 108 ± 2° is realized. Under application of voltage, the surface is charged and becomes increasingly hydrophilic in nature due to variations in surface energy close to the positive electrode (Fig. 3b). This is evidenced by a reduction in the contact angle from 108° to 62° as the applied voltage is increased from 0 to 1000 V (Fig. 3c). The generation of a wettability difference between the two sides of the droplet induces a continuous pulling force, with the entire droplet being driven towards the positive electrode. This complete process is shown in Movie S1. In general terms, wettability is controlled by the magnitude of the applied voltage and the electrode spacing. As can be seen in Fig. 3c, variation of the applied

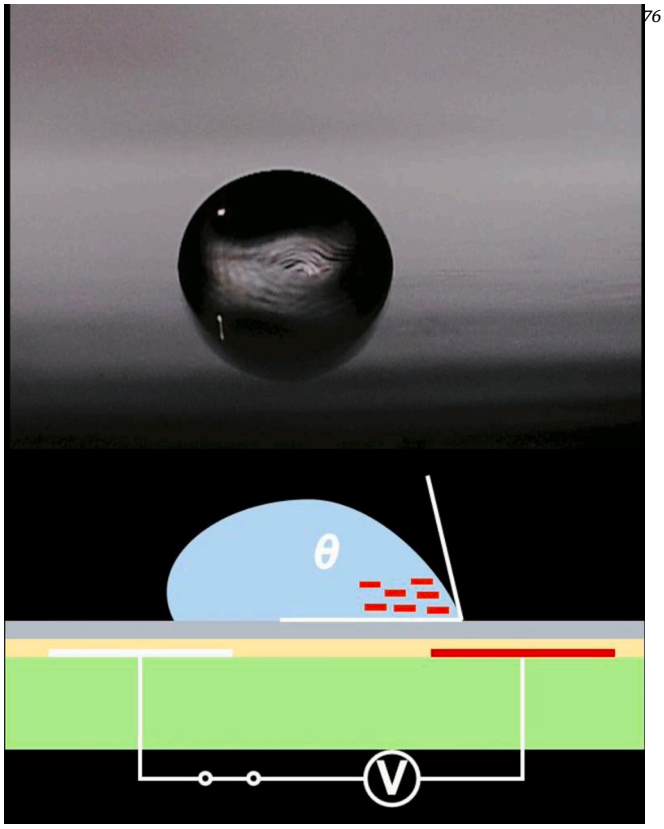

Movie S1. A video clip is available online. Supplementary material related to this article can be found online at doi:10.1016/j.snb.2022.132276.

voltage from 0 V to 1000 V induces a large reduction of 44.5° in the water contact angle, with a minimum water contact angle of 62.5 ± 1.5° at 1000 V. Moreover, and as shown in Fig. 3**c**, a decrease in electrode spacing yields a smaller contact angle.

Fig. 3d,e show the state of the liquid interface at the outlet of the valve before and after application of voltage (1000 V), respectively. It should be noted that an AC voltage is used in all experiments since it minimizes hysteresis effects [38]. Since it's difficult to record the liquid status at the valve area, we use a pressure pump to mimic the driving force and a high-speed camera to record the liquid interface at the valve area (as shown in Fig. S2). Before application of voltage, fluid is held at the outlet of the narrow channel due to surface tension. As soon as the voltage is applied to the valve electrodes, the interface moves forward and along the microfluidic channel. Movie S2 shows the opening of an

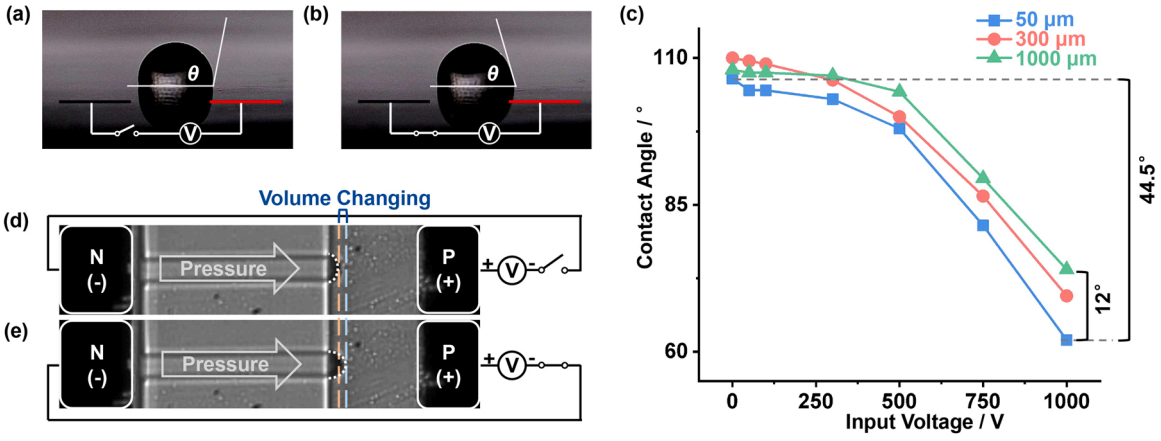

Fig. 3. Measured contact angle of PDMS surface without the application of an electric field (a) and under the application of 1000 V (b). (c) Contact angle of PDMS surface under the application of different voltage and electrode spacing. (d) and (e) Liquid interface at the outlet of the valve without the application of an electric field and under the application of 1000 V.

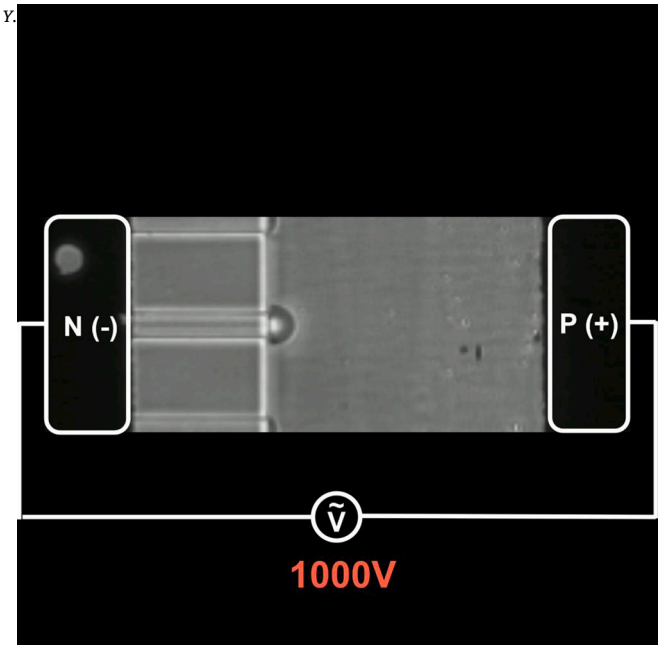

Movie S2. A video clip is available online. Supplementary material related to this article can be found online at doi:10.1016/j.snb.2022.132276.

EWC valve under pressure pump control. Specifically, for an EWC valve and a 10 × 10 μm channel cross section, the threshold pressure is 195 ± 25 mBar without voltage application, and between 40 and 100 mBar when a voltage of 1000 V (50% duty cycle at 10 Hz) is applied. As seen in Movie S2, liquid interface movement is synchronous with the input electric field at 10 Hz. When the input voltage peaks at 1000 V, the liquid-air interface is furthest away from the valve, with the liquid interface returning to its original position when the input voltage decreases to zero due to surface tension. When voltage reaches 1000 V, surface tension is not sufficient to hold the fluid at the outlet, causing the opening of the valve.

We next investigated the dependency of the threshold pressure on electrical and geometric parameters (Fig. 4). To confirm that the pressure pump-based experiments were able to correctly mimic operational conditions within the centrifugal microfluidic platform, calibration experiments (with and without an applied voltage of 1000 V) using both platforms were performed, with the results being presented in Fig. 4a. For these experiments, the liquid plug pressure on the centrifugal microfluidic platform is calculated using Eq. (1), with an electrode spacing, pulse frequency and duty cycle of 100 μm, 10 Hz and 50%, respectively. The EWC valve open data of centrifugal rotation speeds and their equivalent calculated threshold pressures are shown in Table S1. Inspection of Fig. 4a confirms that the threshold pressures are closely matched on both platforms and for all channel cross sections studied.

Fig. 4b reports the threshold pressure of the EWC valve for different channel cross sections and different input voltages with the same electrode spacing, pulse frequency and duty cycle used in the calibration experiments. It can be seen that threshold pressures for 1000 V and 500 V are significantly lower than the corresponding threshold pressures without the application of voltage for all channel cross sections. Conversely, it can be seen that when using a voltage of 200 V, EWC valve operation for larger channel cross sections is compromised. Put simply, application of a higher voltage leads to the generation of a stronger electric field between the electrodes, which in turn leads to a larger increase in surface hydrophilicity and a lower threshold pressure. That means the valve opening is a more robust process.

To further investigate the operation of EWC valves, the electrode spacing was varied between 50 μm and 1000 μm, whilst maintaining the voltage, pulse frequency and duty cycle at 1000 V, 10 Hz and 50%, respectively. As shown in Fig. 4c, the threshold pressure decreases as the electrode spacing decreases, with electrode spacings below 300 μm allowing robust switching between open and closed states. Finally, an assessment of the effect of pulse frequency and duty cycle is shown in Fig. 4d for a voltage of 1000 V and an electrode spacing of 100 μm, with data indicating minimal variation in EWC valve performance.

As noted, centrifugal microfluidic systems should ideally be adept at performing complex assays involving multiple reagents and numerous individual steps [39]. This requires the monolithic integration of multiple valves. To this end, we next fabricated a centrifugal microfluidic device containing two types of EWC valve. As shown in Fig. 5a, the device contains three (reagent) 1.5 μL reservoirs, a 5.5 μL reaction chamber and a 5 μL detection chamber. Loading EWC valves (labeled

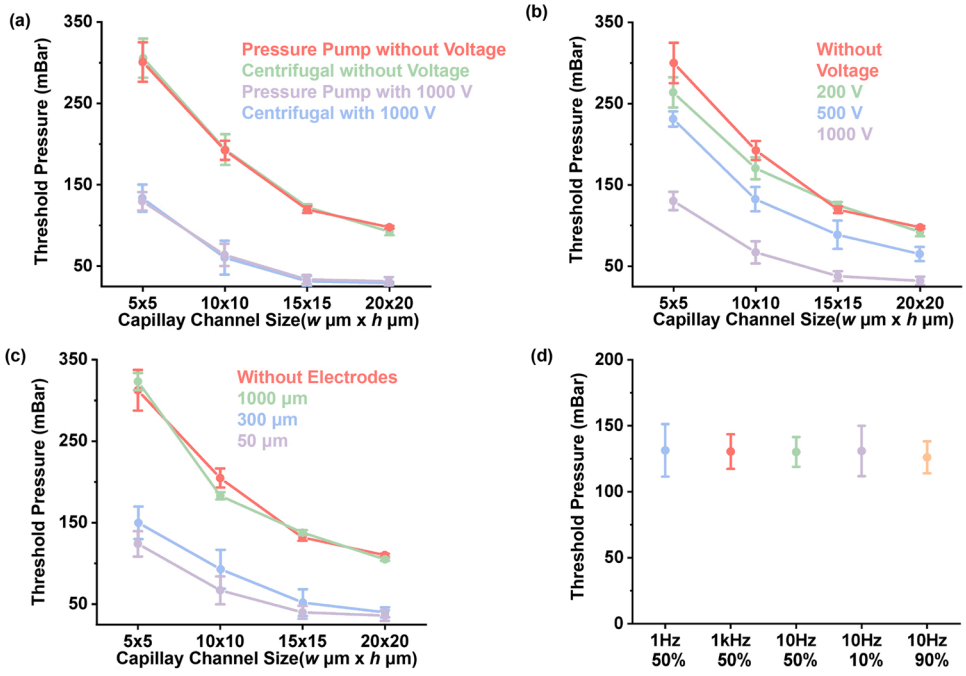

Fig. 4. The dependency of threshold pressure on electrical and geometric parameters. (a) Threshold pressure comparison between the pressure pump-based and the centrifugal microfluidic-based platforms with and without an applied voltage of 1000 V. The electrode spacing is 100 μm and the pulse frequency is 10 Hz, with a duty cycle of 50%. (b) Variation in pressure with voltage between 0 and 1000 V, with an electrode spacing of 100 μm and pulse frequency of 10 Hz, with a duty cycle of 50%. (c) Variation of threshold pressure with electrode spacing between 50 μm and 1000 μm, with a voltage of 1000 V at 10 Hz and a duty cycle of 50%. (d) Variation of threshold pressure with voltage frequency and duty cycle when the electrode spacing is 100 μm and voltage is 1000 V.

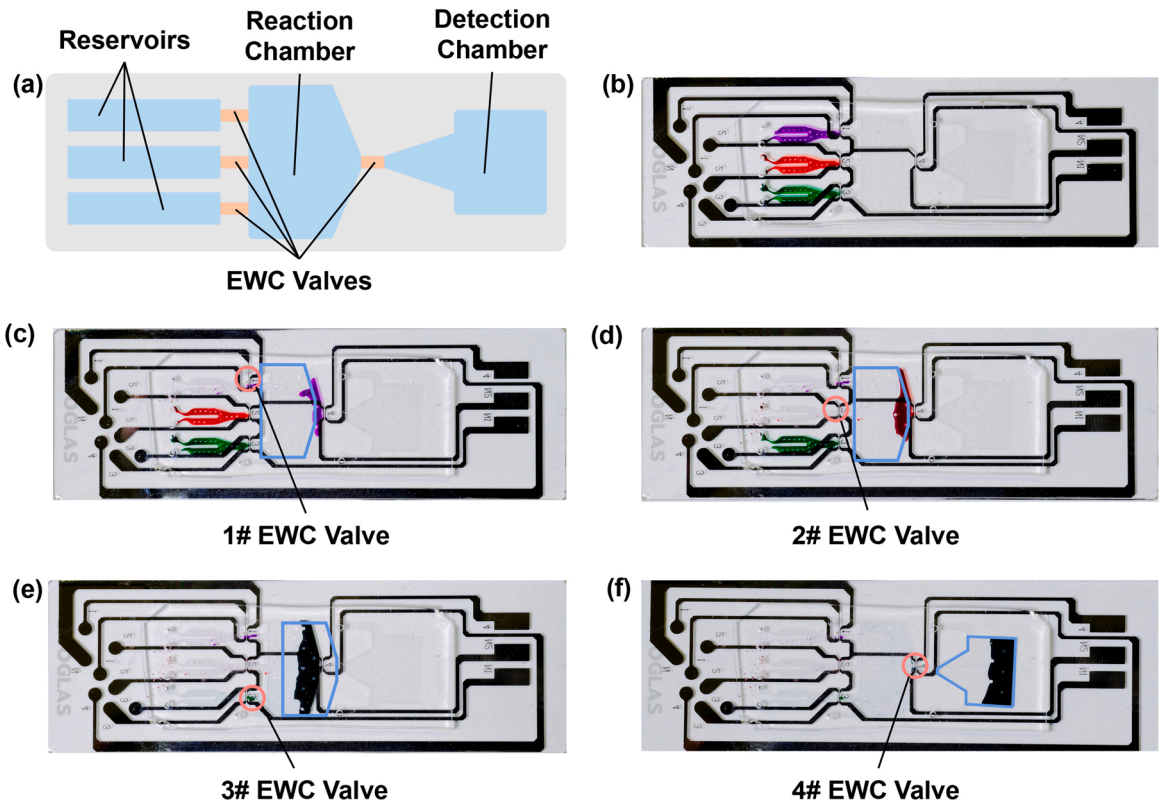

Fig. 5. Sequential multi-step liquid manipulation using EWC valves. (a) Schematic of a centrifugal microfluidic chip containing 4 EWC valves. (b) Three reservoirs are loaded with aqueous solutions (of purple, orange or green food dye) (c), (d) and (e) Application of 1000 V to valves 1#, 2# and 3# to trigger sequential opening at 800 rpm, with the fluid in the corresponding reservoir being pushed into the reaction chamber within 10 s. The entire chip is oscillated by applying clockwise and counterclockwise spinning speed periodically to accelerate fluidic mixing in the reaction chamber. (f) 1000 V is applied to open valve 4# at 1200 rpm, with the mixed fluid being driven into the detection chamber.

1#, 2# and 3#) had a channel cross section of 15 × 15 μm, with R and Δr being equal to 4.5 cm and 1 cm, respectively. The downstream detection valve (labeled 4#) has a channel cross section of 7.5 × 7.5 μm (and thus is able to hold higher pressures), with R and Δr being equal to 6 cm and 0.5 cm, respectively. The system was then used to process fluids as shown in Fig. 5b-f and Movie S3. In brief, the three reservoirs were filled with aqueous solutions of either purple, orange or green food dyes. Rotation of the centrifugal device at 800 rpm for 10 s, drives the fluids in three reservoirs towards valves 1#, 2# and 3#, concurrently removing any trapped air bubbles (Fig. 5b). Sequential application of 1000 V to each valve, causes opening in less than 1 s, with the fluid in the corresponding reservoir being pushed into the reaction chamber at 800 rpm in 10 s (Fig. 5c-e). Finally, 1000 V is applied to valve 4# whilst the centrifugal microfluidic device is rotated at 1200 rpm, causing the mixed fluid to move into the detection chamber (Fig. 5f).

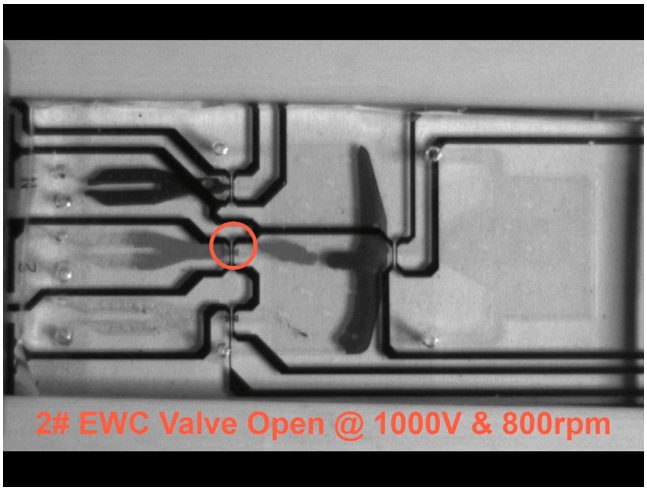

Movie S3. A video clip is available online. Supplementary material related to this article can be found online at doi:10.1016/j.snb.2022.132276.

Finally, to showcase the utility of EWC valves within a centrifugal microfluidic platform, we performed a bead-based fluorescence-linked immunosorbent assay (FLISA). FLISA-based methods combine immunosorbent assays with fluorescent reporters, where antibodies conjugated to a fluorophore are quantified through measurement of time-integrated emission intensities. FLISA-based techniques are well-suited to use in the small volumes associated with microfluidic systems since analytical sensitivities are high and limits of detection low [40]. Specifically, we performed a CD4 antigen-antibody fluorescence-linked immunosorbent assay. Prior to centrifugal manipulation, all the three reagents (CD4 antibody-bound magnetic beads, CD4 cell antigen and fluorophore-conjugated CD4 antibodies) are injected into their respective reservoirs (Fig. 6a). A detailed description of assay procedure is provided in Materials and Methods section. Next, valves 1# and 2# are opened under the application of 1000 V at 800 rpm. This allows CD4 antigen and CD4 antibody-bound magnetic beads to be transferred into reaction chamber and mixed. This is followed by incubation for 1 h at 36 ℃. All reservoirs and the reaction chamber are 50 μm high, so as to allow introduction of a sufficiently large volume of the assay mixture. Under the centrifugal force, the magnetic beads are driven against from the center of the motor due to higher density than the liquid. Since the beads move from the reaction chamber (1.5 μL) to the detection chamber (0.03 μL), the concentration is increased approximately 50 times (Fig. 6b). After the initial incubation, valve 3# is opened under the application of 1000 V at 800 rpm to release fluorophore-conjugated CD4 antibodies into the reaction chamber, as shown in Fig. 6c. After the

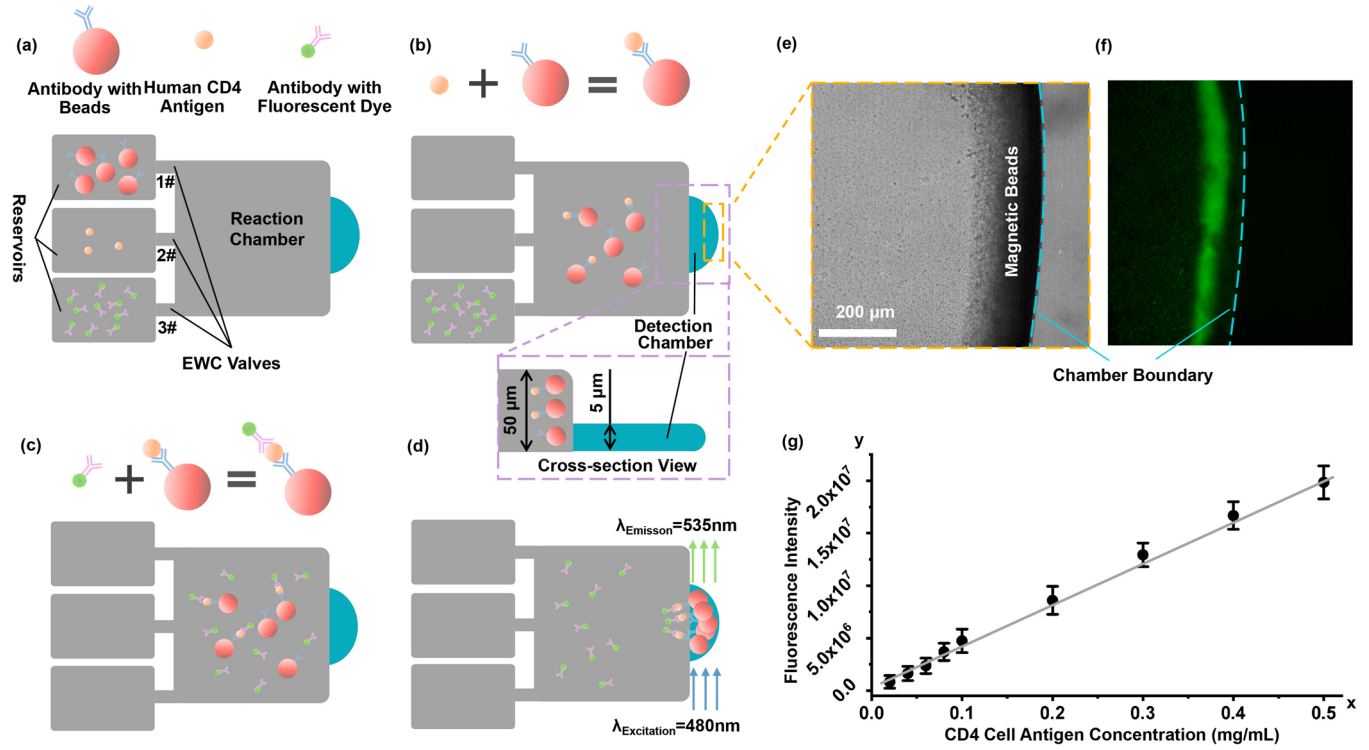

Fig. 6. Bead-based FLISA detection of CD4 human immune cell antigen in a centrifugal microfluidic platform integrating EWC valves. (a) Three reagents (CD4 antibody-bound magnetic beads, CD4 cell antigen and fluorophore-conjugated CD4 antibodies) are injected into their respective reservoirs within the centrifugal microfluidic device. (b) Valves 1# and 2# are opened under the application of 1000 V at 800 rpm to allow CD4 antigen and CD4 antibody-bound magnetic beads to enter the reaction chamber for incubation and CD4 antigen capture by magnetic beads. (c) Valve 3# is opened under the application of 1000 V at 800 rpm to release fluorophore-conjugated CD4 antibodies into reaction chamber, with the liquid being incubated for 1 h after mixing. Subsequently, fluorescently labeled antibody is bound to the target protein. (d) Magnetic beads are collected in the detection chamber by increasing the rotational speed to 2500 rpm. (e) Brightfield image of magnetic beads within the detection chamber. (f) Fluorescence image of magnetic beads within the detection chamber. (g) Variation of fluorescence intensity with CD4 antigen concentration (from 0.02 to 0.5 mg/mL).

second incubation, the magnetic beads are transferred into the detection chamber and collected by increasing the rotational speed to 2500 rpm, and detected using fluorescence microscopy (Fig. 6d). The images shown in Fig. 6e,f show the magnetic beads within the detection chamber and their fluorescence emission after the antigen-antibody reaction. This confirms that the magnetic beads are bound to fluorophore-conjugated CD4 antibodies, with the fluorescence intensity reporting CD4 cell antigen concentration. To further assess assay performance, fluorescence intensities for CD4 antigen concentrations between 0.02 and 0.5 mg/mL were measured under identical experimental conditions and are shown in Fig. 6g. Despite the simplicity of the employed FLISA method, results demonstrate the utility of EWC valves in performing immunosorbent assays within microliter-volume centrifugal formats. In this regard, it is important to note that the centrifugal FLISA platform ensures both sensitive and rapid analysis, whilst removing the cumbersome washing steps associated with conventional ELISA-based methods.

4. Conclusions

Herein, we have presented a new type of electrowetting valve for use in centrifugal microfluidic systems. In simple terms, the EWC valve holds liquid within a narrow microfluidic channel adjacent to a geometric expansion and opens upon application of an electric field to surface-mounted electrodes. Significantly, the valves are controlled wirelessly via a WiFi-integrated PCB, and thus can be used to perform bespoke and complex fluid manipulations. Compared with the passive valves, the electric wetting mechanism increases the control flexibility on individual valves. Additionally, EWC valves are appreciably smaller than previously reported active valves based on mechanical, optical or chemical membrane deformation, with large numbers being easily integrated within a single centrifugal device. A key advantage of the developed platform is the fact that the centrifugal microfluidic device does not need to stop during operating to control valve status. Parallel operation on multi valves also becomes possible benefitting from the decoupling between trigging stimuli and disc spinning. The utility of EWC valves in biological experimentation was additionally highlighted through the quantification of CD4 human immune cell antigen concentration with a limit of detection of 0.04 mg/mL. Finally, since the integration of electrodes into the microfluidic device is both simple and inexpensive, EWC valves considerably enhance the operational and configurational flexibility of centrifugal microfluidic platforms, improving fluid control and enabling complex chemical and biological workflows to be performed with ease.

CRediT authorship contribution statement

Yanming Xia: Conceptualization, Methodology, Software, Validation, Formal analysis, Investigation, Writing, Visualization. **Chao Song:** Methodology, Validation, Formal analysis, Investigation. **Yingchao Meng:** Investigation. **Peng Xue:** Investigation. **Andrew J. deMello:** Resources, Writing, Supervision. **Quan Gao:** Conceptualization. **Stavros Stavrakis:** Writing. **Shenglin Ma:** Methodology, Validation, Resources, Writing, Supervision. **Xiaobao Cao:** Conceptualization, Methodology, Software, Validation, Formal analysis, Investigation, Writing, Supervision.

Declaration of Competing Interest

The authors declare that they have no known competing financial

interests or personal relationships that could have appeared to influence the work reported in this paper.

Acknowledgments

The authors would like to thank Dr. Minghan Hu for assistance with contact angle measurements and Prof. Qian Liu and Prof. Zhi Luo for editing. This work was supported by .

Appendix A. Supplementary material

Supplementary data associated with this article can be found in the online version at doi:10.1016/j.snb.2022.132276.

References

[1] K.S. Elvira, X. Casadevall i Solvas, R.C. Wootton, A.J. deMello, The past, present and potential for microfluidic reactor technology in chemical synthesis, Nat. Chem. 5 (2013) 905–915.
[2] O. Strohmeier, M. Keller, F. Schwemmer, S. Zehnle, D. Mark, F. von Stetten, et al., Centrifugal microfluidic platforms: advanced unit operations and applications, Chem. Soc. Rev. 44 (2015) 6187–6229.
[3] R. Gorkin, J. Park, J. Siegrist, M. Amasia, B.S. Lee, J.M. Park, et al., Centrifugal microfluidics for biomedical applications, Lab Chip 10 (2010) 1758–1773.
[4] G.N. Hortobagyi, Charles M. Balch, MD: accomplishments in academic leadership, Lab Chip 20 (2009) 1548–1555.
[5] H. Kido, A. Maquieira, B.D. Hammock, Disc-based immunoassay microarrays, Anal. Chim. Acta 411 (2000) 1–11.
[6] J. Siegrist, R. Gorkin, M. Bastien, G. Stewart, R. Peytavi, H. Kido, et al., Validation of a centrifugal microfluidic sample lysis and homogenization platform for nucleic acid extraction with clinical samples, Lab Chip 10 (2010) 363–371.
[7] F. Schuler, F. Schwemmer, M. Trotter, S. Wadle, R. Zengerle, F. von Stetten, et al., Centrifugal step emulsification applied for absolute quantification of nucleic acids by digital droplet RPA, Lab Chip 15 (2015) 2759–2766.
[8] H. Cho, H.Y. Kim, J.Y. Kang, T.S. Kim, How the capillary burst microvalve works, J. Colloid Interface Sci. 306 (2007) 379–385.
[9] Y.J. Chang, Y.T. Lin, C.C. Liao, Chamfer-type capillary stop valve and its microfluidic application to blood typing tests, SLAS Technol. 24 (2019) 188–195.
[10] M. Bauer, M. Ataei, M. Caicedo, K. Jackson, M. Madou, L. Bousse, Burst valves for commercial microfluidics: a critical analysis, Microfluid. Nanofluid 23 (2019) 1–12.
[11] H. Hwang, H.H. Kim, Y.K. Cho, Elastomeric membrane valves in a disc, Lab Chip 11 (2011) 1434–1436.
[12] D.H. Kang, N.K. Kim, S.W. Park, W. Lee, H.W. Kang, A microfluidic circuit consisting of individualized components with a 3D slope valve for automation of sequential liquid control, Lab Chip 20 (2020) 4433–4441.
[13] L. Swayne, A. Kazarine, E.J. Templeton, E.D. Salin, Rapid prototyping of pneumatically actuated hydrocarbon gel valves for centrifugal microfluidic devices, Talanta 134 (2015) 443–447.
[14] Y. Kim, S.N. Jeong, B. Kim, D.P. Kim, Y.K. Cho, Rapid and automated quantification of microalgal lipids on a spinning disc, Anal. Chem. 87 (2015) 7865–7871.
[15] M.S. Woolf, L.M. Dignan, H.M. Lewis, C.J. Tomley, A.Q. Nauman, J.P. Landers, Optically-controlled closable microvalves for polymeric centrifugal microfluidic devices, Lab Chip 20 (2020) 1426–1440.
[16] J.L. Garcia-Cordero, D. Kurzbuch, F. Benito-Lopez, D. Diamond, L.P. Lee, A. J. Ricco, Optically addressable single-use microfluidic valves by laser printer lithography, Lab Chip 10 (2010) 2680–2687.
[17] R. Gorkin 3rd, C.E. Nwankire, J. Gaughran, X. Zhang, G.G. Donohoe, M. Rook, et al., Centrifugo-pneumatic valving utilizing dissolvable films, Lab Chip 12 (2012) 2894–2902.
[18] M.M. Aeinehvand, P. Magaña, M.S. Aeinehvand, O. Aguilar, M.J. Madou, S. O. Martinez-Chapa, Ultra-rapid and low-cost fabrication of centrifugal microfluidic platforms with active mechanical valves, RSC Adv. 7 (2017) 55400–55407.
[19] M.M. Aeinehvand, R.F. Martins Fernandes, M.F. Jiménez Moreno, V.J. Lara Díaz, M. Madou, S.O. Martinez-Chapa, Aluminium valving and magneto-balloon mixing for rapid prediction of septic shock on centrifugal microfluidic platforms, Sens. Actuators B Chem. 276 (2018) 429–436.
[20] M.M. Aeinehvand, F. Ibrahim, S.W. Harun, A. Kazemzadeh, H.A. Rothan, R. Yusof, et al., Reversible thermo-pneumatic valves on centrifugal microfluidic platforms, Lab Chip 15 (2015) 3358–3369.
[21] H. Wu, Y. Chen, Q. Yang, C. Peng, X. Wang, M. Zhang, et al., A reversible valve-assisted chip coupling with integrated sample treatment and CRISPR/Cas12a for visual detection of Vibrio parahaemolyticus, Biosens. Bioelectron. 188 (2021), 113352.
[22] Z. Cai, J. Xiang, B. Zhang, W. Wang, A magnetically actuated valve for centrifugal microfluidic applications, Sens. Actuators B Chem. 206 (2015) 22–29.
[23] Z. Cai, J. Xiang, W. Wang, A pinch-valve for centrifugal microfluidic platforms and its application in sequential valving operation and plasma extraction, Sens. Actuators B Chem. 221 (2015) 257–264.
[24] Z. Cai, J. Xiang, H. Chen, W. Wang, Membrane-based valves and inward-pumping system for centrifugal microfluidic platforms, Sens. Actuators B Chem. 228 (2016) 251–258.
[25] J. Xiang, Z. Cai, Y. Zhang, W. Wang, Wedge actuated normally-open and normally-closed valves for centrifugal microfluidic applications, Sens. Actuators B Chem. 243 (2017) 542–548.
[26] J. Xiang, Z. Cai, Y. Zhang, W. Wang, Mechanically programmed valving technology and the active flow switching application in centrifugal microfluidics, Sens. Actuators B Chem. 259 (2018) 325–331.
[27] T.H. Kim, V. Sunkara, J. Park, C.J. Kim, H.K. Woo, Y.K. Cho, A lab-on-a-disc with reversible and thermally stable diaphragm valves, Lab Chip 16 (2016) 3741–3749.
[28] T.-H. Kim, C.-J. Kim, Y. Kim, Y.-K. Cho, Centrifugal microfluidic system for a fully automated N-fold serial dilution, Sens. Actuators B Chem. 256 (2018) 310–317.
[29] W.R. Rodriguez, N. Christodoulides, P.N. Floriano, S. Graham, S. Mohanty, M. Dixon, et al., A microchip CD4 counting method for HIV monitoring in resource-poor settings, PLoS Med. 2 (2005), e182.
[30] N. Ford, G. Meintjes, M. Vitoria, G. Greene, T. Chiller, The evolving role of CD4 cell counts in HIV care, Curr. Opin. HIV AIDS 12 (2017) 123–128.
[31] Y.-J. Chang, S.-C. Chen, C.-L. Hsu, Study on microchannel design and burst frequency detection for centrifugal microfluidic system, Adv. Mater. Sci. Eng. 2013 (2013) 1–9.
[32] T.-S. Leu, P.-Y. Chang, Pressure barrier of capillary stop valves in micro sample separators, Sens. Actuators A Phys. 115 (2004) 508–515.
[33] W. Satoh, H. Yokomaku, H. Hosono, N. Ohnishi, H. Suzuki, Electrowetting-based valve for the control of the capillary flow, J. Appl. Phys. 103 (2008) 1–9.
[34] T. Mérian, F. He, H. Yan, D. Chu, J.N. Talbert, J.M. Goddard, et al., Development and surface characterization of an electrowetting valve for capillary-driven microfluidics, Colloids Surf. A Physicochem. Eng. Asp. 414 (2012) 251–258.
[35] C.K. Koo, F. He, S.R. Nugen, An inkjet-printed electrowetting valve for paper-fluidic sensors, Analyst 138 (2013) 4998–5004.
[36] F. He, S.R. Nugen, Automating fluid delivery in a capillary microfluidic device using low-voltage electrowetting valves, Microfluid. Nanofluid. 16 (2014) 879–886.
[37] L. Clime, D. Brassard, M. Geissler, T. Veres, Active pneumatic control of centrifugal microfluidic flows for lab-on-a-chip applications, Lab Chip 15 (2015) 2400–2411.
[38] I. Nagiel, AC Electrowetting Actuation of Droplets on a Digital Microfluidic Platform, Duke University, 2007.
[39] R. Gorkin, L. Clime, M. Madou, H. Kido, Pneumatic pumping in centrifugal microfluidic platforms, Microfluid. Nanofluid. 9 (2010) 541–549.
[40] R.R. Soares, P. Novo, A.M. Azevedo, P. Fernandes, M.R. Aires-Barros, V. Chu, et al., On-chip sample preparation and analyte quantification using a microfluidic aqueous two-phase extraction coupled with an immunoassay, Lab Chip 14 (2014) 4284–4294.

Yanming Xia is currently a Ph.D. candidate in Department of Mechanical & Electrical Engineering, Xiamen University. He was a Visiting Scholar in Institute of Chemical and Bioengineering, ETH Zürich from 2019 to 2021. His main research interest is focused on the valve controlling of microfluidic platforms and non-Si MEMS fabrication process development.

Chao Song holds a Bachelor's degree in Material Science and Engineering from Shandong University and a Master's degree in Chemistry from Tsinghua University. He is currently a Ph.D. student in the Department of Chemistry and Applied Biosciences from ETH Zurich.

Yingchao Meng is a Ph.D. student at the Institute of Chemical and Bioengineering, ETH Zürich. His main research interest is development of microfluidic platforms for extracellular vesicle separation and rare cell enrichment.

Peng Xue holds a Bachelor's degree in Biology from Northwest University, China, a Master's degree in Molecular biology from Beijing Normal University, China and a Ph.D. degree in Biochemistry and Molecular Biology from Institute of Biophysics, Chinese Academy of Sciences, Beijing, China. He was a visiting scientist and Postdoctoral researcher in ETH from 2017 to 2020. He is currently a senior researcher in Institute of Biophysics. He has significant experience in detection and identification of ultra-low abundance proteins. His current research interesting is focus on single cell proteome with the microfluidic systems.

Andrew J. deMello is currently Professor of Biochemical Engineering in the Department of Chemistry and Applied Biosciences at ETH Zurich. Prior to his arrival in Zurich he was Professor of Chemical Nanosciences and Head of the Nanostructured Materials and Devices Section in the Chemistry Department at Imperial College London. His research interests cover a broad range of activities in the general area of microfluidics and nanoscale science. Primary specializations include the development of microfluidic devices for high-throughput biological and chemical analysis, ultra-sensitive optical detection techniques, nanofluidic reaction systems for chemical synthesis, novel methods for nanoparticle synthesis, the exploitation of semiconducting materials in diagnostic applications, the development of intelligent microfluidics and the processing of living organisms.

Quan Gao graduated from Northwestern Polytechnical University with a bachelor's degree in engineering in 2019. From 2019 to 2021, he completed his master's degree at NPU and ETH Zurich (deMello Group). He is currently a doctorate student at ETH Zurich's Multi-Scale Robotics Lab. His current research mainly focuses on micro-robotics and surgical robotics.

Stavros Stavrakis received his B.Sc. in Chemistry from the University of Crete (Greece) in 1999. In 2005 he gained his Ph.D. in Biophysical Chemistry from the University of Crete working on time-resolved vibrational spectroscopy of cytochrome oxidases. Prior to moving to Zurich in 2011 he was in the group of Prof. Stephen Quake at Stanford University as a Marie Curie fellow where he performed research on the development of new optical tools to improve the throughput of current single molecule DNA sequencing platforms. As a Marie Curie postdoctoral fellow, he also worked in Dr. David McGloin's lab at the University of Dundee, dealing with optical trapping of single cells in microfluidic chips. His current research interests are focused on applications of single molecule fluorescence detection, and optofluidics in biology.

Shenglin Ma is Associate Professor in the Department of Mechanical and Electrical Engineering at Xiamen University, China. He received his Ph.D. from Peking University and has also been a guest researcher with the National Key Laboratory of Science and Technology in Micro/Nano Fabrication at Peking University. His research focuses on TSV based 3D integration technology, MEMS and its applications.

Xiaobao Cao is a senior scientist in the Department of Chemistry and Applied Biosciences at ETH Zurich. He received his Ph.D. from ETH and continued his Postdoc at ETH. His research focuses on developing microfluidic tools for high-throughput screening and single cell analysis.